Kinetic Insight into the Electrochemical Lithium Insertion Process in the Puckered-Layer γ'-V2O5 Polymorph

Rita Baddour-Hadjean, Marianne Safrany Renard, Jean Pierre Pereira-Ramos

Kinetic insight into the electrochemical lithium insertion process in the puckered-layer γ'-V_2O_5 polymorph

R. Baddour-Hadjean*, M. Safrany Renard, J.P. Pereira-Ramos

ICMPE (UMR 7182), CNRS, UPEC, 2 rue Henri Dunant, 94320 Thiais, France

**corresponding author: baddour@icmpe.cnrs.fr*

Abstract

Cycling properties, rate capability performance and kinetic parameters for Li insertion in the puckered γ'-V_2O_5 host lattice are reported here in the 4.0 V- 2.5 V voltage window corresponding to $0 \leq x \leq 1$ in γ-$Li_xV_2O_5$. Whereas a high reversible behaviour and good cycling performance are achieved (135 mAh g^{-1} after 50 cycles at C/10), the rate capability study shows a rapid increase in the discharge-charge hysteresis with the current density, impeding the recovering of high capacity values even at C/2 rate. The kinetics of the electrochemical lithium insertion reaction in γ'-V_2O_5 has been investigated by ac impedance spectroscopy and discussed in the light of the structural mechanism. The chemical diffusion coefficient D_{Li} is found constant in the $0 \leq x < 0.4$ biphasic region while lithium ions more rapidly diffuse in the solid solution domain $0.4 \leq x \leq 1$ with greater D_{Li} values by one or two orders of magnitude (around 10^{-9} cm^2 s^{-1}). An increase in charge transfer resistance and cathode impedance characterizes nevertheless the second part of the discharge. These findings explain the limitations in the reaction kinetics in the micrometric γ'-V_2O_5 cathode material and give directions toward improved performance.

Keywords: γ'-V_2O_5, cathode material, kinetics, Li diffusion, AC impedance spectroscopy

Introduction

The α-V_2O_5 polymorph was among the first transition metal oxide identified as Li intercalation compounds [1]. Its interest stems from a layered structure made of V_2O_5 sheets with Van der Waals interactions between oxide planes promoting facile insertion reactions. In addition, the presence of 2 V^{5+} ions allows a high capacity to be reached, i. e. ≈ 150 mAh g^{-1} and 300 mAh g^{-1} obtained for $0 < x \leq 1$ (3.5 V - 2.5 V potential window) and $0 < x \leq 2$ (3.5 V - 2.3 V potential window), respectively. Quite logically its possible application as cathode material in secondary Li batteries and Li-ion batteries prompted many researchers to work on the electrochemical properties of α-V_2O_5 [1-10] with a special focus on the associate structural behaviour [4, 6-18]. Some results emerging from these works have allowed to establish the $Li_xV_2O_5$ phase diagram with $0 < x < 2$ in which the successive emergence of more or less distorted lithiated phases is described [2, 4, 7-9, 18]. In addition, the Li transport kinetics in this canonical intercalation host lattice has been deeply investigated as a function of x in $Li_xV_2O_5$ [19-25].

Recent studies based on DFT calculations have outlined the interest of metastable phases obtained from topochemical removal of cations from the appropriate $M_xV_2O_5$ bronzes (M = Li, Cu, Ag) [26, 27]. A higher open circuit voltage combined with lower diffusion barriers are predicted as specific features of such cation-free metastable phases. Among the V_2O_5 polymorphs, the γ'-V_2O_5 has been firstly mentioned to coexist with α-V_2O_5 after a discharge-charge cycle in the 3.8 V-2.15 V potential range [8, 28, 29]. This γ'-V_2O_5 polymorph is indeed the charge product of the highly puckered γ-LiV_2O_5 phase irreversibly produced upon discharge at 2.3 V. Its formation is responsible for a voltage enhancement of ≈ 0.2 V related to the presence of two additional voltage plateaus at 3.6 V and 3.5 V upon cycling [8]. However, even when the chemical synthesis of γ'-V_2O_5 was early proposed [28], only its lithiated γ-LiV_2O_5 has been investigated as positive electrode material for Li-ion batteries [29-35]. Various synthesis ways of γ-LiV_2O_5 were used such as carbothermal reduction at 600°C [30], precipitation reaction [31], hydrothermal or solvothermal routes [32-34], sol-gel templating route [35] leading to controversial and scattered results especially in the large 4 V-2 V window.

Surprisingly, the interest in the γ'-V_2O_5 polymorph toward insertion reactions has been firstly illustrated in the case of sodium insertion [36-39]. Indeed, sodium is reversibly accommodated in γ'-V_2O_5 at a high working voltage of 3.3 V vs Na^+/Na, remarkably at the

same energy level as lithium insertion [36]. The strong puckering of the oxide layers in γ'-V_2O_5 probably promotes insertion reactions compared to the α-V_2O_5 form. It is one of the reasons for considering the γ'-polymorph as an interesting candidate as cathode material for Li batteries.

The electrochemical and structural study of γ'-V_2O_5 toward Li insertion has been very recently reported [40]. A detailed XRD and Raman spectroscopy study allowed to establish the complete phase diagram of the Li/γ'-V_2O_5 system in the widest 4.00 V- 2.15 V voltage window. This pioneering work unveiled the interest of the corrugated γ'-V_2O_5 framework to accommodate a large amount of Li ions (up to 2 Li/mole of oxide). The typical discharge exhibits two pairs of well-defined reversible steps at 3.58/3.47 V and 2.42/2.36 V separated by a sharp potential drop of about 1 V. A strong influence of the depth of discharge on the cycling performance was outlined [40]. In the widest 4.00 V- 2.15 V voltage window ($0 < x \leq 1.94$), a high capacity of 285 mAh g^{-1} was reported. However, severe capacity fading upon cycling was observed in this voltage range due to the emergence of the fully lithiated ζ-$Li_{\approx 2}V_2O_5$ phase at 2.36 V. By reducing the voltage limits to 4.0 V- 2.4 V region ($0 < x \leq 1.3$), an attractive capacity of 185 mAh g^{-1} was reached, but still associated to a continuous capacity fading. Furthermore, the sharp potential drop of 1 V around x = 1 constitutes another important drawback in the 4.0 V- 2.4 V voltage range.

The present paper focuses on the electrochemical properties of γ'-V_2O_5 in the high voltage window corresponding to the exchange of 1 Li^+/mole of oxide (147 mAh g^{-1}). Cycling properties, rate capability behaviour and kinetics parameters for Li insertion in γ'-V_2O_5 are reported here in the 4.0 V - 2.5 V voltage window. The kinetic data are discussed at the light of the structural mechanism recently evidenced for γ'-V_2O_5.

Experimental

γ'-V_2O_5 is obtained by chemical oxidation of γ-LiV_2O_5 synthesized by the carbothermal reduction method [30]. A solution of NO_2BF_4 (solid Alfa Aesar 96%) in acetonitrile, molar ratio 1:4, allows the complete Li removal from the γ-LiV_2O_5 host structure. The solution is maintained under stirring at room temperature for 24h. After reaction and decantation, the supernatant liquid is removed by pipetting. After three successive washing steps with

acetonitrile, the powder is then vacuum dried at 70°C for 24h. The powder color changing from black to orange confirms the complete lithium deintercalation. Electrochemical titration and chemical redox titration confirmed the 5+ oxidation state of vanadium in γ'-V_2O_5.

Two-electrode coin cells (CR 2032) with lithium disk as reference and auxiliary electrodes were used to perform electrochemical studies. γ'-V_2O_5 positive electrode was prepared by mixing 80 wt % of active material, 7.5 wt% of acetylene black, 7.5 wt% of graphite and 5wt% of teflon as binder agent. About 10 mg of this mixture was pressed on a stainless steel grid (14 mm diam., 0.35 mm thick) under a pressure of 5 tons per cm^2. The separator consists of three glass Whatman microfiber filters soaked by a solution of 1M $LiClO_4$ in propylene carbonate (PC) as electrolyte. All the coin cells were assembled in an argon-filled glove box where water and oxygen concentrations were kept less than 1 ppm. Electrochemical experiments were performed at ambient temperature using a VMP3 Biologic apparatus.

Impedance measurements were carried out in conventional three electrode cells under argon atmosphere. The cell was filled with 1M $LiClO_4$ in propylene carbonate (PC). The positive electrode was made of the active material in the same manner as the composite electrode used in coin cell for cycling and rate capability experiments. Reference and counter electrodes were made of Li wires in separate compartments filled up with electrolyte. The working electrode composition was changed by coulometric titration using a low current density corresponding to a C/20 rate. Equilibrium was considered as reached when the open circuit voltage remained stable (< 0.2 mV for 1h). A discharge curve performed at very low rate (C/100) is considered as the OCV curve. Impedance measurements were performed in the frequency range 4×10^4 to 0.5×10^{-3} Hz with a VMP3 Biologic Multipotentiostat-Galvanostat apparatus. The excitation signal was 10 mV peak to peak. All these electrochemical measurements were performed in an argon-filled glove box.

XRD measurements were performed using a Panalytical X'pert pro diffractometer equipped with an X'celerator detector and a Co Kα radiation (wavelength λ = 1.7889 Å).

Results and discussion

The X-ray diffraction pattern of the γ'-V_2O_5 powder is shown in **Figure 1**. All the diffraction lines can be indexed on the basis of an orthorhombic symmetry (space group *Pnma*) with the following unit cell parameters: a = 9.95 Å; b = 3.59 Å; c = 10.04 Å. These values are in good accord with those previously reported [28, 36-38]. The γ'-V_2O_5 powder is characterized by a high *00l* preferred orientation corresponding to the stacking of platelets along the *c* axis. SEM micrograph (see inset in **Figure 1**) indicates big aggregates made of platelets of a few µm. The corresponding layered structure is composed of infinite ribbons parallel to the *b* axis made of VO_5 edges-sharing distorted pyramids alternatively up and down, as illustrated in **Figure 2**. These ribbons are linked to each other along the *a*- direction by one corner's oxygen, leading to folded layers laying in the (*ab*) plane and stacked along the *c*- axis.

A typical discharge curve performed at very low current density (C/100) allows to get a quasi-equilibrium voltage-composition curve E vs x in γ-$Li_xV_2O_5$ (**Figure 3**). From the very first lithium ions, the potential rapidly decreases from 4 V to 3.62 V and remains stable near 3.6 V in the $0.02 < x < 0.4$ lithium composition range. Then, a potential decline from 3.6 to 3.55 V is observed for $0.4 < x < 0.5$ followed by a less sloping decrease from 3.55 V to 3.45 V in the $0.5 < x < 0.92$ composition range. For higher Li contents, a sharp potential drop up to 2.5 V leads to the full lithiation of γ'-V_2O_5 into γ-LiV_2O_5. The maximum specific capacity delivered by γ'-V_2O_5 in this voltage window reaches the value of 147 mAh g^{-1}.

The discharge-charge curves of γ'-V_2O_5 performed at C/10 exhibit a similar profile, consisting in two steps located at 3.58 V and 3.47 V (**Figure 4**). The first discharge process involves a specific capacity of 145 mAh g^{-1}. Then, a quantitative charge process allows the extraction of 1 lithium ion from γ-LiV_2O_5 in two steps located at 3.65 V and 3.52 V, leading to a symmetric charge-discharge profile. The cycling experiments (see inset in **Figure 4**) indicate a high reversible behaviour and a slow capacity decline limited to 6% with still 135 mAh g^{-1} recovered after 50 cycles. This behaviour competes well with the value of 125 mAh g^{-1} reported at C/5 for γ-LiV_2O_5 prepared by the carbothermal reduction method [30] and outperforms the capacities of 100-110 mAh g^{-1} and 57 mAh g^{-1} reported for γ-LiV_2O_5 prepared respectively by a precipitation technique [31] and a direct sol-gel soft templating method [35].

The influence of the C rate on the discharge-charge profile of γ'-V_2O_5 is reported in **Figure 5**. At C/5 and C/10, similar capacities are achieved, i.e. 145 and 140 mAh g^{-1} respectively, and a value of still 130 mAh g^{-1} can be recovered at C/2. However, increasing the current density in the C/2-5C range leads an increase in the polarization (**Figure 5a**). The hysteresis value of 200 mV at C/2 greatly increases with higher current densities, which impedes the recovering of high efficiency when the C rate exceeds 1C: discharge capacities of 100, 80 and 40 mAh g^{-1} are obtained at C, 2C and 5C respectively (**Figure 5b**). These findings suggest some kinetic limitations occur and prompted us to examine in details the electrochemical kinetics of Li insertion into γ'-V_2O_5.

The typical AC impedance diagrams obtained for γ-$Li_xV_2O_5$ electrodes are reported in **Figure 6**. The conventional equivalent circuit developed for intercalation compounds was used [41].Two kinds of Nyquist diagrams can be observed. For $0 < x \leq 0.6$ (**Figure 6a**), all the spectra practically superimpose, showing a well-defined charge transfer semi-circle centered at 130-160 Hz followed by a straight line with a phase angle of 45° up to 0.5 mHz corresponding to the Warburg region (when $\omega >> 2D_{Li}/L^2$, L being the maximum length of the diffusion pathway) [41]. For higher Li contents, i.e. $0.6 < x \leq 1$, all the diagrams superimpose again but no reliable Warburg region can be defined (**Figure 6b**). Instead, the well-defined high frequency semi-circle is followed by a quasi-vertical line corresponding to the finite diffusion ($\omega << 2D_{Li}/L^2$). This behaviour reveals a faster Li diffusion in the richest Li composition range. Another discrepancy concerns the lower value of the characteristic frequency of charge transfer, of 100 Hz in the $0.6 < x \leq 1$ composition range vs. 160-130 Hz for $0 < x \leq 0.6$. Finally, the cathode impedance is significantly larger in the second half of the discharge.

The main kinetic parameters of the Li insertion reaction into γ'-V_2O_5 like the cathode impedance $|Z|$, the charge transfer resistance R_{ct} and the double layer capacitance C_{dl} are reported in **Figure 7** as a function of the Li content x. A crucial difference is seen between the two composition ranges for the cathode impedance : $|Z|$ slightly decreases with x between 180 and 140 Ω for $x \leq 0.6$ but then strongly increases by a factor 2 for $x > 0.6$ and more to reach 475 Ω for γ-LiV_2O_5 (**Figure 7a**). As seen from **Figure 7b**, the charge transfer resistance R_{ct} remains constant around ≈ 55 Ω in the first half of the Li insertion process ($0 < x \leq 0.4$) with an exchange current density of 0.46 mA cm^{-2}, in line with usual j° values found for other

transition metal oxides [20, 25, 41, 42]. This constant R_{ct} value corresponds to a biphasic region where γ'-V_2O_5 and γ-$Li_{0.4}V_2O_5$ coexist [40]. For $x > 0.5$, the kinetics of charge transfer is however progressively slowed with further lithiation, as indicated by the continuous R_{ct} increase to reach 75 Ω for γ-LiV_2O_5 ($j° = 0.34$ mA/cm^2). The double layer capacitance C_{dl} remains stable, around 18 µF cm^{-2} in the first part of the discharge, to reach 24 µF cm^{-2} in the second half (**Figure 7c**).

These electrochemical results have been interpreted in the light of the structural data recently reported during the electrochemical Li insertion in γ'-V_2O_5 [40]. It was shown that the discharge-charge profile in the $0 < x \leq 1$ composition range corresponds to a two phase behaviour for $0 < x < 0.4$ followed by a wide single phase γ-$Li_xV_2O_5$ domain for $0.4 \leq x \leq 1$. These structural changes are associated to a weak unit cell volume expansion of only 4%. Clearly, the present study evidences a change in the cathode impedance $|Z|$, the charge transfer resistance R_{ct} and the double layer capacitance C_{dl} in the second half of the discharge, i.e. from $x \approx 0.5$. This change in the kinetic parameters characterizes the Li enrichment of the γ-$Li_{0.4}V_2O_5$ phase according to a solid solution behaviour to progressively reach the γ-LiV_2O_5 phase [40]. The C_{dl} increase can be explained by the slight volume expansion of the active material of a few percent, leading to a moderate increase in the electrochemical surface area. The significant increase in both the charge transfer resistance and electrode impedance suggests that the growing V^{4+}/V^{5+} ratio disadvantages the rate of charge transfer, because of a decrease in the electronic conduction. Such an assumption is supported by the crystallographic data reported for the two types of vanadium environment available in the Li-free γ'-V_2O_5 phase and the lithiated γ-LiV_2O_5 phase [39, 40]. Indeed, V_aO_5 and V_bO_5 pyramids volumes are similar in γ'-V_2O_5 (4.461 Å^3 and 4.531 Å^3, respectively), due to the presence of V^{5+} ions in both polyhedra. Conversely, in γ-LiV_2O_5, different values of respectively 4.675 Å^{3}and 5.114 Å^3 account for the existence of V^{5+} ions in V_aO_5 pyramids and V^{4+} ions in V_bO_5 pyramids. This highly localized electron character highlighted in γ-LiV_2O_5 is well correlated with the highest cathode impedance and charge transfer resistance values observed for the $x = 1$ composition. Then, the upward trend of both parameters with x suggests a progressive increase in the electron localization with the V^{4+}/V^{5+} ratio.

A reliable evaluation of the apparent lithium diffusion coefficient D_{Li} has been achieved over the whole $0 < x \leq 1$ lithium composition range. In the first part of the discharge ($0 < x \leq 0.6$),

a Warburg domain can be reliably defined (see inset in **Figure 6a**). The numerical values of D_{Li} have been calculated from the analysis of the Warburg impedance plotted in the complex plane:

-Im Z or Re Z = $A_w \omega^{-1/2}$, using equation (1) [41]:

$$A_w = V_M.(dE/dx)_x / F\sqrt{2}\, S\, D_{Li}^{1/2} \qquad \omega >> 2D_{Li}/L^2 \qquad \text{(eq 1)}$$

A_w is the Warburg prefactor, V_M is the molar volume of the compound (V_M= 53.9 $cm^3.mol^{-1}$), S is the geometric surface area of the electrode (1 cm^2), $(dE/dx)_x$ is the slope, at fixed x, of the equilibrium potential composition curve (**Figure 3**).

For $0.6 < x \leq 1$, D_{Li} has been calculated from the limiting low frequency resistance R_L, using equation (2) [41]:

$$R_L = (V_m/nFS)\,(dE/dx)\,(L/3D_{Li}) \qquad \omega << 2D_{Li}/L^2 \qquad \text{(eq 2)}$$

L is the maximum length of the diffusion pathway, estimated to a few µm from SEM images, i.e, $L \approx 1.5\ 10^{-4}$ cm. R_L is graphically determined from the intersection of the low frequency asymptote with the real axis after subtraction of electrolyte and charge transfer resistances (see inset in **Figure 6b**). R_L values of 24, 12, 13 and 8 Ω are found for respectively x = 0.7, 0.8, 0.9 and 1.

The resulting D_{Li} values in the $0 < x \leq 1$ composition range are plotted in **Figure 8**. The lowest D_{Li} values are found at the beginning of the reaction for $0 < x \leq 0.3$ around 10^{-12} $cm^2\ s^{-1}$, i.e. practically in the γ'-V_2O_5 /γ-$Li_{0.4}V_2O_5$ biphasic region. Then, as soon as the first member of the monophasic region is formed (x = 0.4), Li transport is significantly promoted with values in the range 10^{-10}-10^{-9} $cm^2\ s^{-1}$ in spite of higher Li contents (x = 0.4, 0.5 and 0.6). In the second half of the discharge, the disappearance of the Warburg region at the benefit of the quasi-vertical line of the finite diffusion highlights a much faster diffusion kinetics. Assuming a L value of ≈ 1.5 µm, D_{Li} is found to still increase from $2.4\ 10^{-10}$ to $4.3\ 10^{-9}$ $cm^2\ s^{-1}$ from x = 0.7 to x = 1. The order of magnitude between the two sets of data should be at least of one decade given the comparison of extrapolated limiting frequencies: in the order of 10^{-3} Hz when $0.1 \leq x \leq 0.6$ against a few dozen of mHz when $0.7 \leq x \leq 1$.

D_{Li} appears as constant in the biphasic region, i.e. when $x < 0.4$ while lithium ions more rapidly diffuse in the single-phase region $0.4 \leq x \leq 1$. It is worth noticing the present D_{Li} evolution evidenced for the puckered γ'-V_2O_5 host lattice contrasts with the more complex variations of lithium diffusivity reported for the parent α-V_2O_5 oxide [6, 19-21, 23, 24]. This

discrepancy can be related to the emergence of successive distorted phases during Li insertion in α-V_2O_5 in the same $0 < x \leq 1$ composition range.

The higher Li diffusivity evidenced in the second part of the discharge indicates that the capacity decline observed at higher C rate (**Figure 4**) could not be ascribed to diffusional limitations but mainly to large cathode impedance and slowdown in the charge transfer kinetics. Improvement of the rate capability must therefore comprise the optimization of these two parameters. Substitutional or interstitial cation incorporation in γ'-V_2O_5 could be envisioned to enhance the electronic conductivity. Combined with appropriate mastering of the particle size and morphology, such strategies should allow optimizing the charge transfer rate and taking advantage of the high Li mobility highlighted in γ'-V_2O_5.

Conclusion

The electrochemical properties of the puckered γ'-V_2O_5 polymorph toward Li insertion are reported here in the high voltage window corresponding to the exchange of 1 Li^+/mole of oxide (4.0 V - 2.5 V). The corresponding specific capacity of 147 mAh g^{-1} is interestingly available at a higher working voltage than α-V_2O_5 (+ 0.2 V). Two well-defined steps at 3.6 V and 3.5 V account for the formation of the lithiated γ-LiV_2O_5 phase. A good cycle life is achieved at C/10 rate with still 130 mAh g^{-1} recovered after 50 cycles. In addition, the rate capability is satisfactory with specific capacities of 100 mAh g^{-1} and 80 mAh g^{-1} at C and 2C rates, respectively. The kinetic parameters for the electrochemical Li insertion reaction have been investigated using AC impedance measurements. A reliable determination of the chemical diffusion coefficient is made over the whole $0 \leq x \leq 1$ lithium composition range, using either the Warburg domain or the limiting resistance. This study highlights the diffusion rate is slower in the first half of the discharge ($x < 0.4$) corresponding to a diphasic region while the solid solution domain ($0.4 < x \leq 1$) is characterized by higher D_{Li} values by one or two orders of magnitude (around 10^{-9} cm^2 s^{-1}). In the second part of the discharge, the kinetics of the reaction is however impeded by a slowdown in the electron transfer kinetics, as illustrated by the increase in charge transfer resistance R_{ct} and cathode impedance. The highly localized electron character in γ-LiV_2O_5 accounts probably for the highest cathode impedance and charge transfer resistance values observed for the $x = 1$ composition. The kinetic behaviour revealed in this work for γ'-V_2O_5 differs from that of the unfolded parent α-V_2O_5

277 oxide showing large and complex D_{Li} variations. Such discrepancy originates probably from
278 different structural mechanisms upon lithiation of the two polymorphs, i.e. minimal structural
279 changes involving a large solid solution domain for the puckered-layered V_2O_5 polymorph vs.
280 successive phase transitions toward distorted ε- and δ -$Li_xV_2O_5$ for α-V_2O_5. Further efforts
281 made in direction of particle size mastering and morphology have already allowed a great
282 enhancement in the rate capability performance. These results will be published very soon.

283

Figure captions

Figure 1. X-ray diffraction pattern of γ'-V_2O_5. Inset: SEM micrograph of the γ'-V_2O_5 powder

Figure 2. Crystal structure of γ'-V_2O_5

Figure 3. Discharge curve of γ'-V_2O_5 at low current density (C/100 rate)

Figure 4. Discharge-charge curves of γ'-V_2O_5 in the 4.00 V- 2.50 V potential range. C/10 rate

Figure 5. Influence of the C rate on the discharge-charge profiles of γ'-V_2O_5 (a) Discharge capacity as a function of the C-rate (b). C/10-5C range

Figure 6. AC impedance diagrams for γ-$Li_xV_2O_5$ electrodes (a) $0 \leq x \leq 0.6$; (b) $0.7 \leq x \leq 1$

Figure 7. Evolution of the cathode impedance $|Z|$ (a), the charge transfer resistance R_{ct} (b) and the double layer capacitance C_{dl} (c) in γ-$Li_xV_2O_5$ ($0 < x \leq 1$).

Figure 8. Evolution of the apparent chemical diffusion coefficient of lithium D_{Li} as a function of x in in γ-$Li_xV_2O_5$. The double dashed line separates the composition domain in which D_{Li} has been determined using either eq (1) or eq (2).

References

[1] M.S. Whittingham, *Chem. Rev*. **104**, 4271 (2004).

[2] D. W. Murphy, P. A. Christian, F. J. Disalvo, J. V. Waszczak, *Inorg. Chem*. **18**, 2800 (1979).

[3] J. P. Pereira-Ramos, R. Messina, C. Piolet, J. Devynck, *Electrochim. Acta*. **33**, 1003 (1988).

[4] C. Delmas, H. Cognac-Auradou, J. M. Cocciantelli, M. Menetrier, J. P. Doumerc, *Solid State Ionics* **69**, 257 (1994).

[5] K. West, B. Zachau-Christiansen, T. Jacobsen, S. Skaarup, *Solid State Ionics* **76**, 15 (1995).

[6] Y. Sato, T. Asada, H. Tokugawa, K. Kobayakawa, *J. Power Sources* **68**, 674 (1997).

[7] P. G. Dickens, S. J. French, A. T. Hight, M. F. Pye, *Mater. Res. Bull*. **14**, 1295 (1979).

[8] J. M. Cocciantelli, J. P. Doumerc, M. Pouchard, M. Broussely, J. Labat, *J. Power Sources* **34**, 103 (1991).

[9] R. Baddour-Hadjean, A. Marzouk, J. P. Pereira-Ramos, *J. Raman Spectrosc*. **43**, 153 (2012).

[10] D. Huo, A. Contreras, B. Laïk, P. Bonnet, K. Guérin, D. Muller-Bouvet, C. Cenac-Morthe, R. Baddour-Hadjean, J. P. Pereira-Ramos, *Electrochim. Acta* **245**, 350 (2017).

[11] B. Pecquenard, D. Gourier, N. Baffier, *Solid State Ionics* **78**, 287 (1995).

[12] E. Prouzet, C. C. D. Moulin, F. Villain, A. Tranchant,, *J. Chem. Soc. Faraday Trans*. **92**, 103 (1996).

[13] P. Rozier, J. M. Savariault, J. Galy, *Solid State Ionics* **98**, 133 (1997).

[14] P. Rozier, J. M. Savariault, J. Galy, C. Marichal, J. Hirschinger, P. Granger, *Eur. J. Solid State Inorg. Chem*. **33**, 1 (1996).

[15] J. M. Savariault, P. Rozier, *Phys. B.* **234**, 97 (1997).

[16] R. J. Cava, A. Santoro, D. W. Murphy, S. M. Zahurak, R. M. Fleming, P. Marsh, R. S. Roth, *J. Solid State Chem*. **65**, 63 (1986).

[17] H. Katzke, M. Czank, W. Depmeier, S. Van Smaalen, *Philos. Mag B-Physics Condens. Matter Stat. Mech. Electron. Opt. Magn. Prop.* **75**, 757 (1997).

[18] X. Rocquefelte, F. Boucher, P. Gressier, G. Ouvrard, *Chem. Mater.* **15**, 1812 (2003).

[19] J. P. Pereira-Ramos, R. Messina, J. Perichon, *Solid State Ionics* **40/41**, 974 (1990).

[20] J. Farcy, R. Messina, J. Perichon, *J. Electrochem. Soc*., **137**, 1337 (1990).

[21] S. I. Pyun, J. S. Bae, *Electrochim. Acta* **41**, 919 (1996).

[22] C. Navone, R. Baddour-Hadjean, J. P. Pereira-Ramos, R. Salot, *Electrochim. Acta* **53**, 3329 (2008).

[23] D.Y. Yoo, I. H. Yeo, W. I. Cho, Y. Kang, S. I. Mho, *Analytical Sciences* **29**, 1083 (2013).

[24] Y. Luo, L. R. De Jesus, J. L. Andrews, A. Parija, N. Fleer, D. Juarez Robles, P. P. Mukherjee, S. Banerjee, *ACS Appl. Mater. Interfaces* **10**, 30901 (2018).

[25] D. Huo, B. Laïk, P. Bonnet, K. Guérin, R. Baddour-Hadjean, J. P. Pereira-Ramos, *Electrochim. Acta* **253**, 472 (2017).

[26] A. Parija, D. Prendergast, S. Banerjee, *ACS Appl. Mater. Interfaces* **9**, 23756 (2017).

[27] A. Parija, Y. Liang, J.L. Andrews, L.R. De Jesus, D. Prendergast, S. Banerjee, *Chem. Mater.* **28**, 5611 (2016).

[28] J. M. Cocciantelli, P. Gravereau, J. P. Doumerc, M. Pouchard, P. Hagenmuller, *J. Solid State Chem.* **93**, 497 (1991).

[29] J. M. Cocciantelli, M. Menetrier, C. Delmas, J. P. Doumerc, M. Pouchard, P. Hagenmuller, *Solid State Ionics* **50**, 99 (1992).

[30] J. Barker, M. Y. Saidi, J. L. Swoyer, *J. Electrochem. Soc.* **150**, A1267 (2003).

[31] J. Dai, S. F. Y. Li, Z. Gao, K. S. Siow, *Chem. Mater.* **11**, 3086 (1999).

[32] W. Wang, H. Wang, S. Liu, J. Huang, *J. Solid State Electrochem.* **16**, 2555 (2012).

[33] Y. W. Wang, H. Y. Xu, H. Wang, Y. C. Zhang, Z. Q. Song, H. Yan, C. R. Wan, *Solid State Ionics* **167**, 419 (2004).

[34] N. Li, H, Gong, Y. Qian, *Chin. J. Chem. Phys*., **26**, 597 (2013).

[35] S. Caes, J. C. Arrebola, N. Krins, P. Eloy, E. M. Gaigneaux, C. Henrist, R. Cloots, B. Vertruyen, *J. Mater. Chem. A*., **2**, 5809 (2014).

[36] M. Safrany Renard, N. Emery, R. Baddour-Hadjean, J.P. Pereira-Ramos, *Electrochim. Acta* **252C**, 4 (2017).

[37] M. Safrany Renard, N. Emery, E. M. Roginskii, R. Baddour-Hadjean, J. P. Pereira-Ramos, *J. Solid State Chem*. **254**, 62 (2017).

[38] R. Baddour-Hadjean, L.T. Huynh, N. Emery, J.P. Pereira-Ramos , *Electrochim. Acta* **270**, 129 (2018).

[39] N. Emery, R. Baddour-Hadjean, D. Batyrbekuly, B. Laïk, Z. Bakenov, J. P. Pereira-Ramos, *Chem. Mater*. **30**, 5305 (2018).

[40] R. Baddour-Hadjean, M. Safrany Renard, J.P. Pereira-Ramos, *Acta Mater*. **165**, 183 (2019).

[41] C. Ho, I. D. Raistrick, R.A. Huggins, *J. Electrochem. Soc*., **127**, 343 (1980).

[42] B. Garcia, J. Farcy, J. P. Pereira-Ramos, N. Baffier, *J. Electrochem. Soc*., **144**, 1179 (1997).

Figures

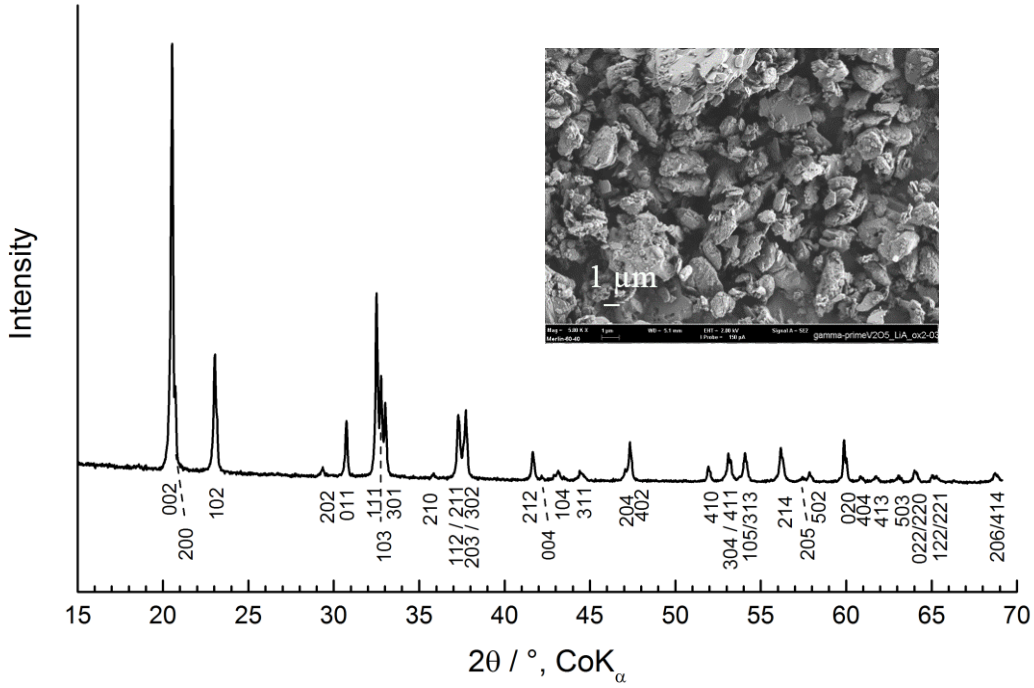

Figure 1. X-ray diffraction pattern of γ'-V_2O_5. Inset: SEM micrograph of the γ'-V_2O_5 powder

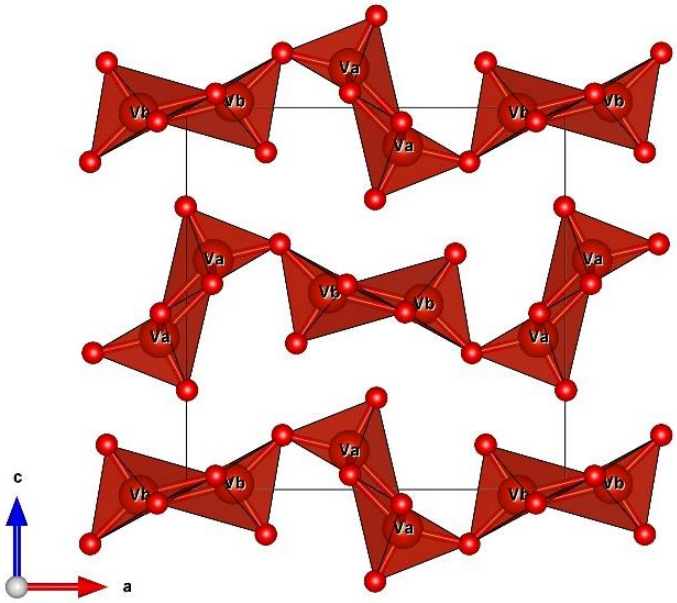

Figure 2. Crystal structure of γ'-V_2O_5

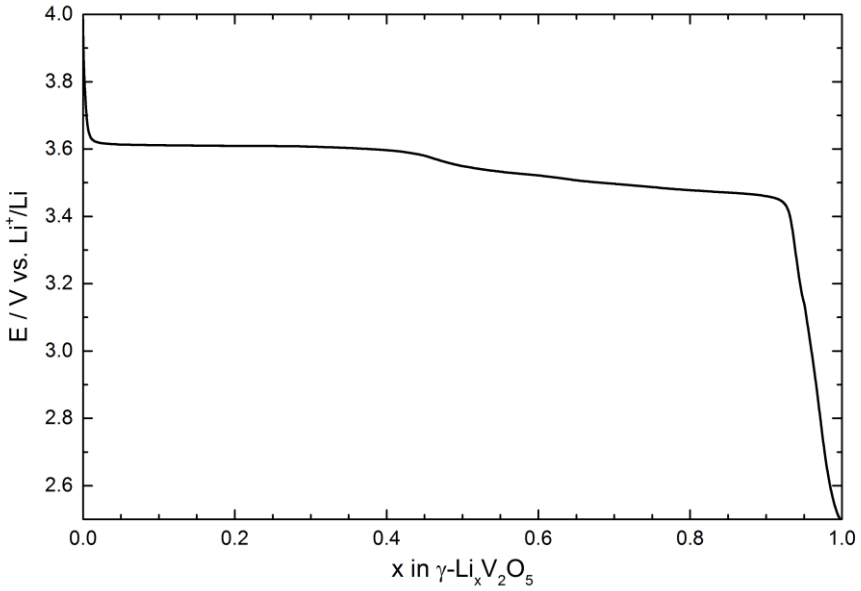

Figure 3. Discharge curve of γ'-V_2O_5 at low current density (C/100 rate)

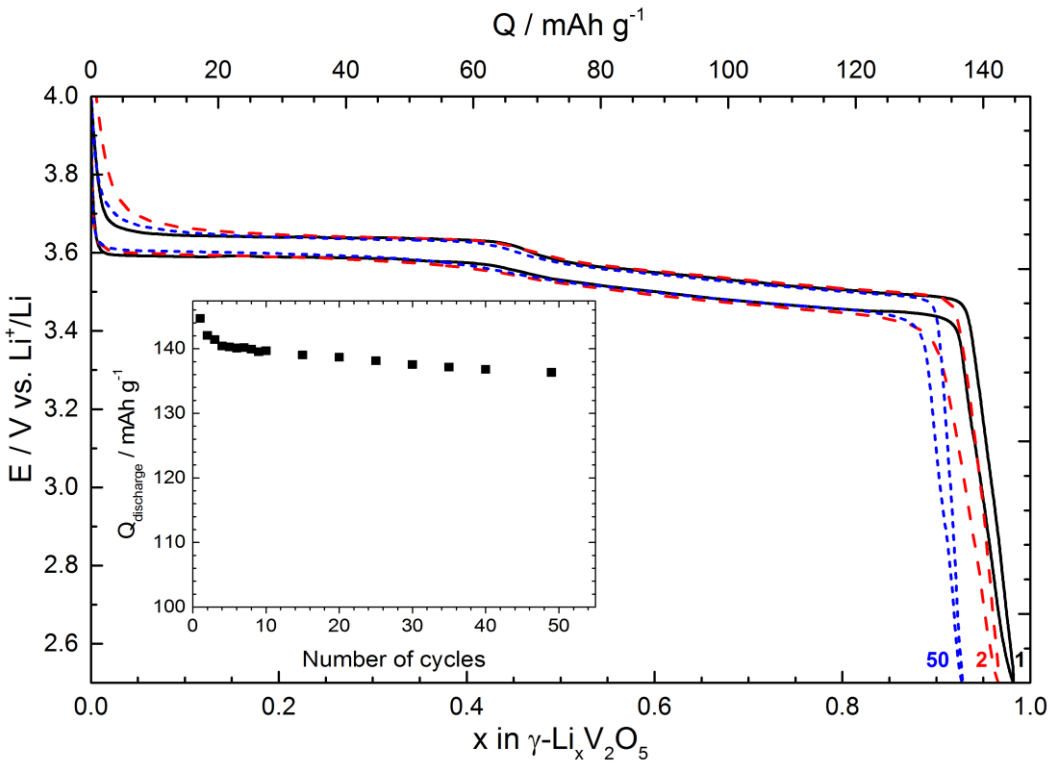

Figure 4. Discharge-charge curves of γ'-V_2O_5 in the 4.00 V- 2.50 V potential range. C/10 rate

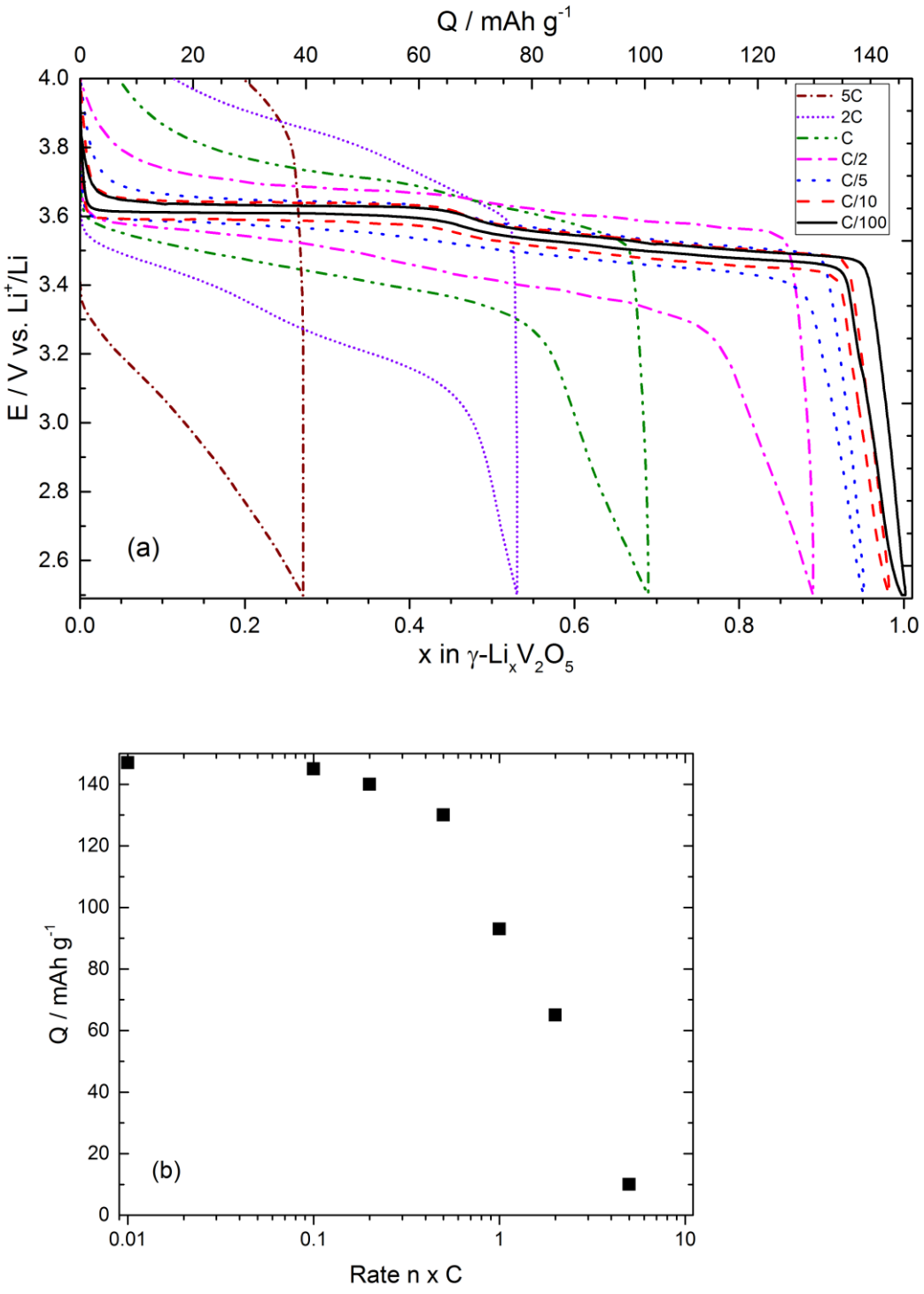

Figure 5. Influence of the C rate on the discharge-charge profiles of γ'-V_2O_5 (a) Discharge capacity as a function of the C-rate (b). C/10-5C range

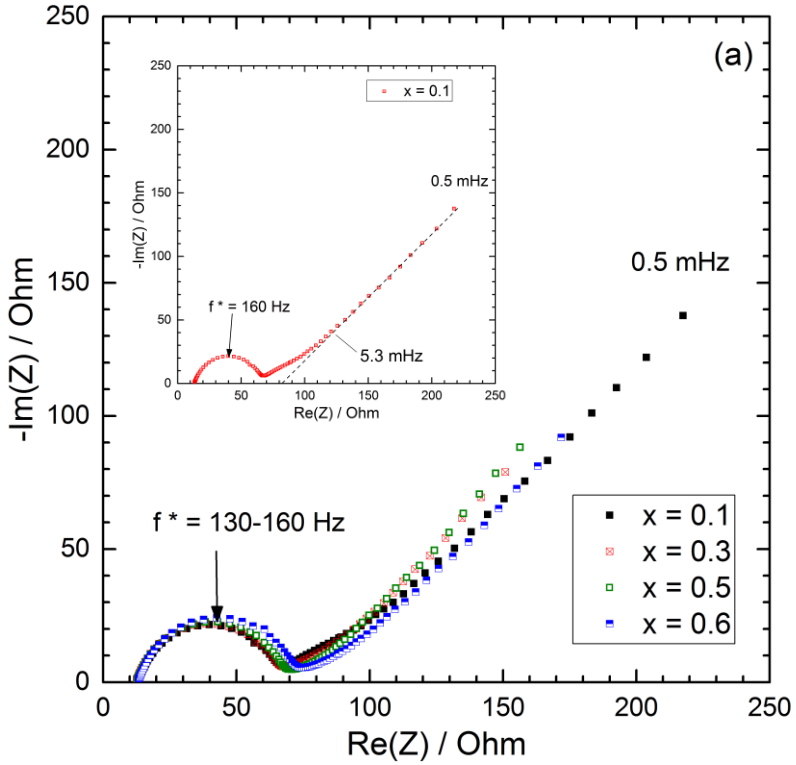

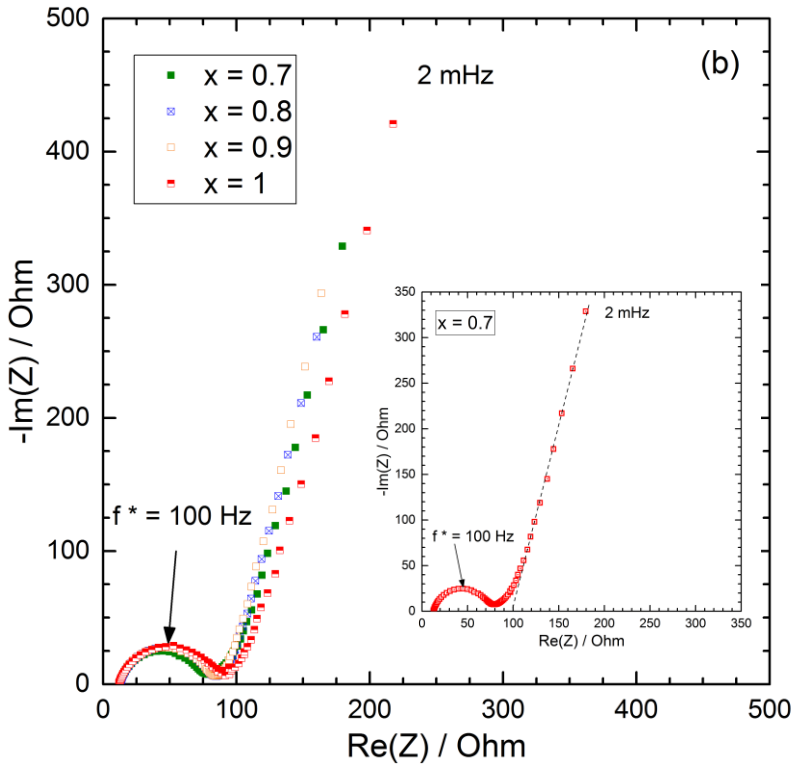

Figure 6. AC impedance diagrams for γ-$Li_xV_2O_5$ electrodes (a) $0 \leq x \leq 0.6$; (b) $0.7 \leq x \leq 1$

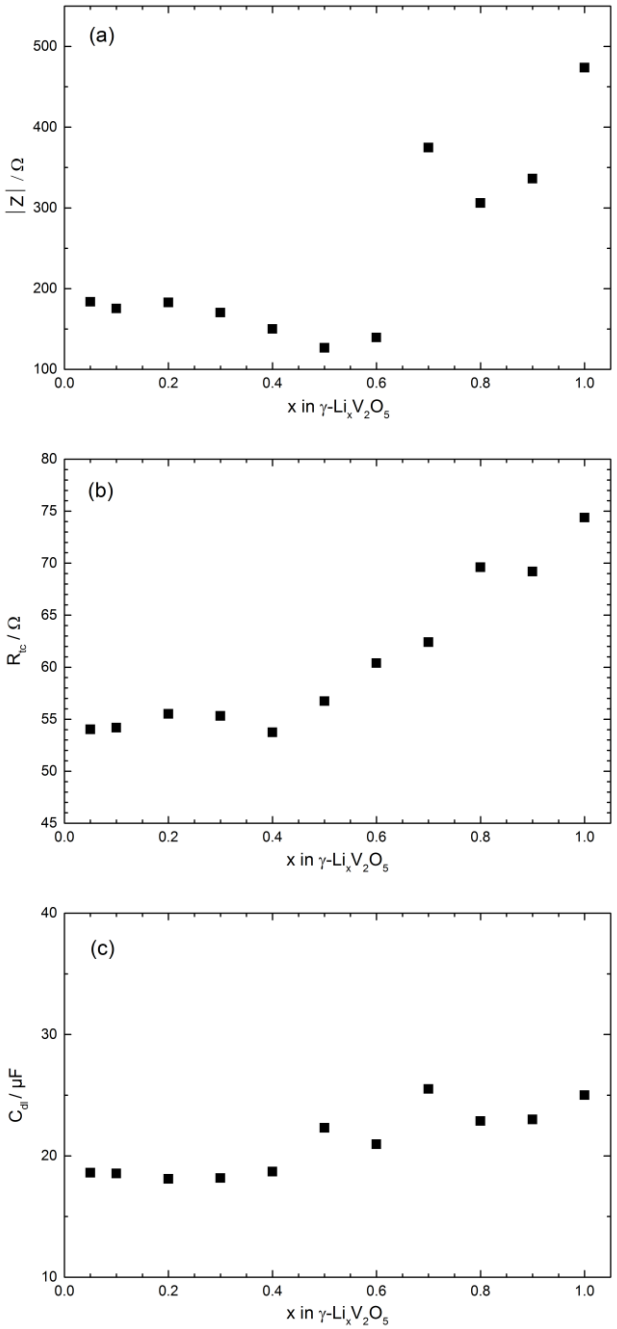

Figure 7. Evolution of the cathode impedance $|Z|$ (a), the charge transfer resistance R_{ct} (b) and the double layer capacitance C_{dl} (c) in γ-$Li_xV_2O_5$ ($0 < x \leq 1$).

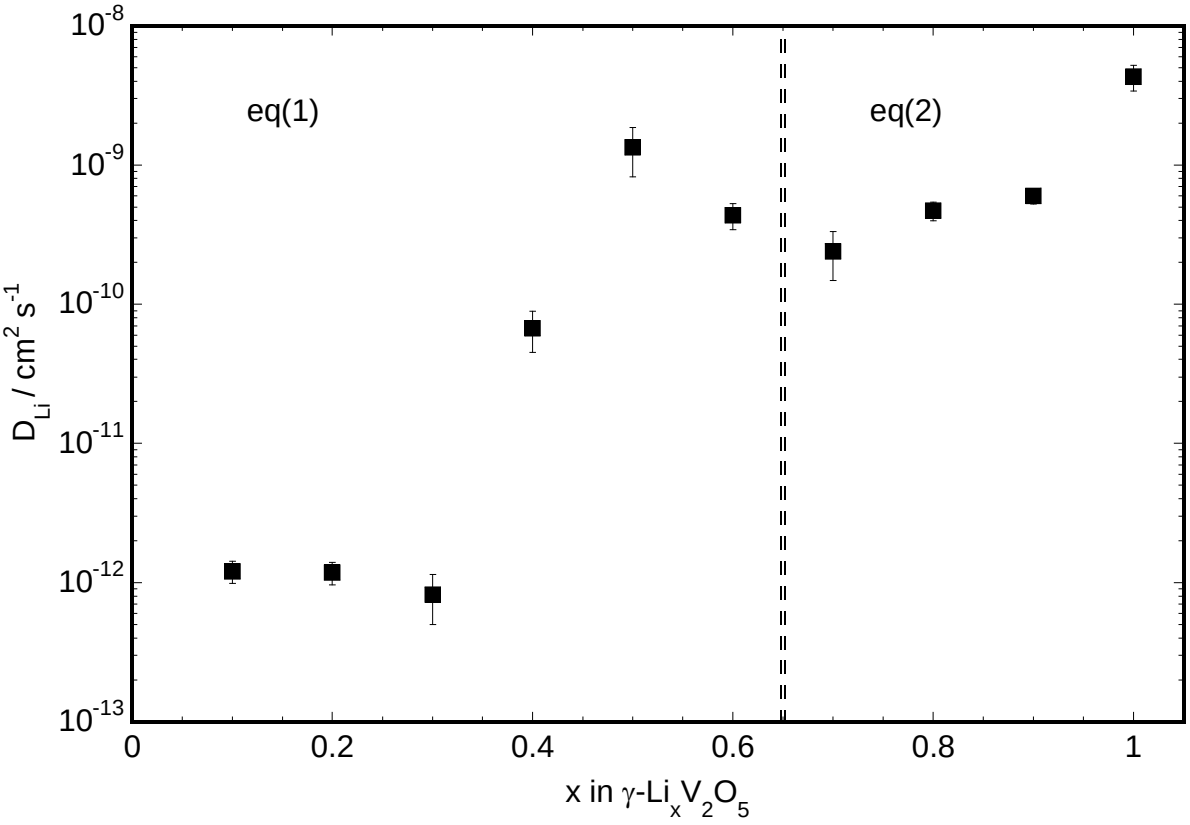

Figure 8. Evolution of the apparent chemical diffusion coefficient of lithium D_{Li} as a function of x in in γ-$Li_xV_2O_5$. The double dashed line separates the composition domain in which D_{Li} has been determined using either eq (1) or eq (2).